Super-detailed FEM simulations for full-scale steel structure with fatal rupture at joints between members-Shaking-table test of full-scale steel frame structure to estimate…

Mizushima, Yasunori

Mukai, Yoichi

Namba, Hisashi

Taga, Kenzo

Saruwatari, Tomoharu

Translated Paper

Super-detailed FEM simulations for full-scale steel structure with fatal rupture at joints between members—Shaking-table test of full-scale steel frame structure to estimate influence of cumulative damage by multiple strong motion: Part 1

Yasunori Mizushima,[1] Yoichi Mukai,[2] Hisashi Namba,[2] Kenzo Taga[2] and Tomoharu Saruwatari[3]

[1]Research & Development Institute, Takenaka Corporation, Chiba, Japan; [2]Department of Architecture, Kobe University, Kobe-shi,Japan; [3]JSOL Corporation, Osaka, Japan

Correspondence
Yasunori Mizushima, Research & Development Institute, Takenaka Corporation, Inzai-shi, Chiba, Japan.
Email: mizushima.yasunori@takenaka.co.jp

Abstract

There have been several studies on analyses using finely meshed finite-element (FE) models to understand in detail the behaviors of buildings during severe earthquakes. The accuracy of such analyses is often validated by comparing the results to the corresponding full-scale shaking-table test. While this approach is highly successful in terms of accuracy, no studies have considered the effect of fractures of members. In this study, numerical analyses are conducted for a steel structure subjected to multiple series of excitations in a full-scale shaking-table test considering fractures. The structure is modeled with planar and solid finite elements, and the fracture is treated by the mandatory deletion of elements at the time at which the fracture is observed in the experiment. The results show that by considering the fracture of steel members with the deletion of elements, the history of input excitations, and the resulting damages, the behaviors can be simulated analytically with a much higher accuracy.

Keywords
detailed model, FEM, full-scale test, shaking-table test, steel structure

1. Introduction

In the conventional structural design of building structures in Japan, the safety of buildings is ensured by adopting moderate members that retain sufficient energy-absorption capacity against expected earthquakes or seismic loadings that are estimated according to the earthquakes. However, in recent years, there have been significant earthquakes beyond the assumed level, and because of societal concerns, the focus has tended to be on unexpected loads due to such earthquakes, especially after the 2011 Tohoku Pacific offshore earthquake. To date, there have been a large number of shaking-table tests at the E-defense of NIED in Japan, and they have been carried out by researchers using specimens that are designed to be full-scale building models; many test cases of large earthquake input motions have been simulated. Those experiments enable the investigation of the ultimate behaviors of building structures from a practical perspective, such as the effects of damaging processes of structural members and of collapsing mechanisms on entire building systems.[1]

At the same time, many numerical simulations have been performed to reproduce the actual structural behaviors observed in shaking-table experiments, and the accuracies of the analyses have been verified. For instance, some numerical simulations for the shaking-table test were conducted for a 4-story full-scale steel building structure at the E-defense.[2–5] In those simulations, various simplified analytical models were used, ie, framing models where column and beam members were considered as beam elements, or locally detailed models using fine finite-element (FE) mesh elements. Hikino and Ohsaki et al. reported the blind analysis contest for the full-scale shaking-table test of the 4-story steel building, and summarized that analytical results can vary extensively according to the differences in analysis conditions among each modeling method or selecting model parameters that depend on each operator.[6,7]

The recent development of high-performance supercomputers enables us to work large-scale calculations by investing large computing resources, so the super-detail meshing FE model analyses can be run for entire building structures. This kind of FE model analysis with mesh generation for the entire building structure aims to solve previously mentioned problems involving varying results; actually, some of the reports show that a very accurate analysis could be obtained by only tuning material model parameters. Yamashita et al. showed that analytical results obtained using a fine, meshed FE model with solid elements agree well with experimental results obtained from the 4-story steel building test.[8] The authors showed analyses for a shaking-table test of a 3-story full-scale steel structure at the E-defense in 2013[9] using a model that were mainly composed of shell elements that are usually used for analysis of steel structures. This model was generated the entire shape of the structural specimen by the fully detailed FE model using fine FE mesh elements. In that study, shell elements that are usually used for analyses of steel structures were mainly used for the model, and by considering analytically the excitation histories of the shaking-table test, they showed that the responses obtained by the analysis agree well with those of the test.[10]

At the same time, the fracture of members is considered as one of the predominant factors that trigger building collapses. In the shaking-table test that was conducted in 2013 for a high-rise steel building structure, it was reported that the fracture of the beam ends caused the collapse of the entire structural frame.[11] In addition, analyses of this shaking-table test were also reported. In their analysis, it was concluded that fracture modeling is important to reproduce the collapse phenomenon.[12] As another example of numerical analysis considering member fractures, Takehara and Nakashima et al. operated numerical simulations for quasi-dynamic loading tests of a full-scale steel structure.[13] However, the analytical models used in those simulations to reproduce the experimental responses were frame models.[12] Thus, these analyses cannot prevent the results-varying problems that depend on modeling or determining model parameters. On the other hand, numerical analyses were utilized for finely meshed FE models for an entire building structure in Refs. [8] and [10]; they did not consider the occurrence of member fractures. Those studies only guaranteed the high accuracy of analyses unless a fracture occurs, but they did not investigate the analytical validity for structural behavior after a fracture occurs.

We carried out finely meshing FE model analyses for full-scale shaking-table tests using a 3-story steel frame structure (details of the test conditions and modeling specification were reported in Ref. [10]). In this paper, we focused on the numerical reproducibility of the post-fracturing behavior in a structural system, such as a rupture at the beam-column connection. In the analysis, the fracture of members is considered by that the elements are eliminated from the model at positions at which the rupture occurred actually. The timings of the eliminations correspond to those of the fracture in the actual experimental results. We also discussed the cumulative damage at the fractured parts. The experimental tests were carried out as a series of multiple vibrating tests to observe the accumulation of damages in the test specimen. Thus, the numerical analysis also considered the sequence of the input history of multiple input motions. Numerical simulations focused on the observed behavior of the nonlinear region in the experiments. This study reports the results of the numerical analyses obtained using the finely meshed FE model, which contains all structural parts of the entire test specimen with shell and solid elements.

2. Shaking-table test

2.1 Specimen of shaking-table test

The entire view of the specimen that was set on the shaking table is shown in Figure 1. The specimen used in the shaking-table test was a full-scale 3-story steel frame. The typical frame plan (on the second floor) and frame elevation (on line B) are displayed in Figure 2. The only object under observation was the frame on the centerline, which is line B, as shown in Figure 2, and it was made as a moment resistant frame. The direction of vibration was along a single axis that was parallel to the X-direction, and the motion in the Y-direction was sufficiently stiffened using brace framing. Columns and beams on the centerline were built with BCR295 and SS400 H-shaped steel, respectively. Dimensions of the columns and beams on line B are listed in Table 1. Frames on lines A and C were designed not to resist horizontal loads. Columns on these lines were provided with hinges at both their top and bottom ends to support only vertical loads. Reinforced concrete slabs were constructed on steel deck plates. The slabs were connected to the beams with a sufficient number of shear-connecting studs with large heads.

In this study, we focused on experimental cases, where the NS-direction component of the observed seismic record at the JR-Takatori station, which was measured during the Hyogoken-Nambu earthquake in 1995 (hereafter, this input motion is referred to as JR-Takatori), was used as the seismic input motion. In those experimental cases, damage was clearly observed on the steel frame. A series of experiments was conducted using seismic input motions from JR-Takatori as well as an artificially generated synthetic input motion to simulate the Nankai-Trough earthquake (Nankai). Nine experimental cases were carried out with an adjusted scale of those input motions for different acceleration levels. Four cases using 40%, 60%, 80%, and 100% (rated for the full-scale acceleration) of the scale of JR-Takatori were considered, and major damage of the test specimen was observed after inputting the loading of JR-Takatori.

2.2 Experimental results

The story-shear force and story-drift ratio relationships obtained from the cases using 40%, 60%, 80%, and 100%
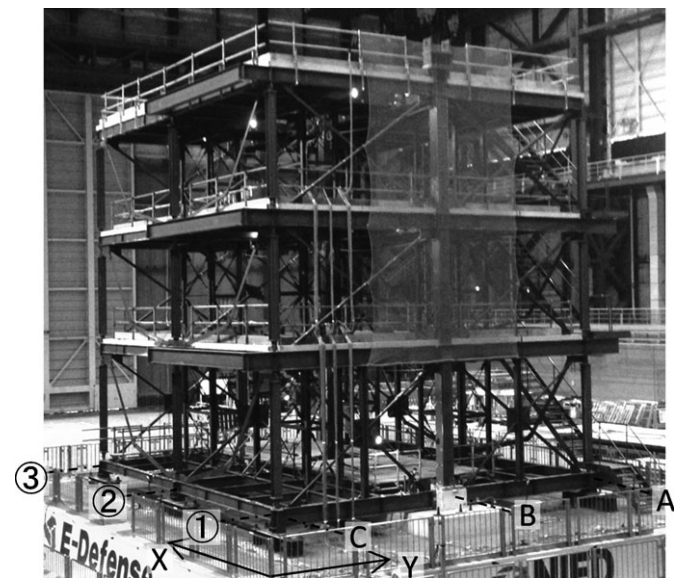

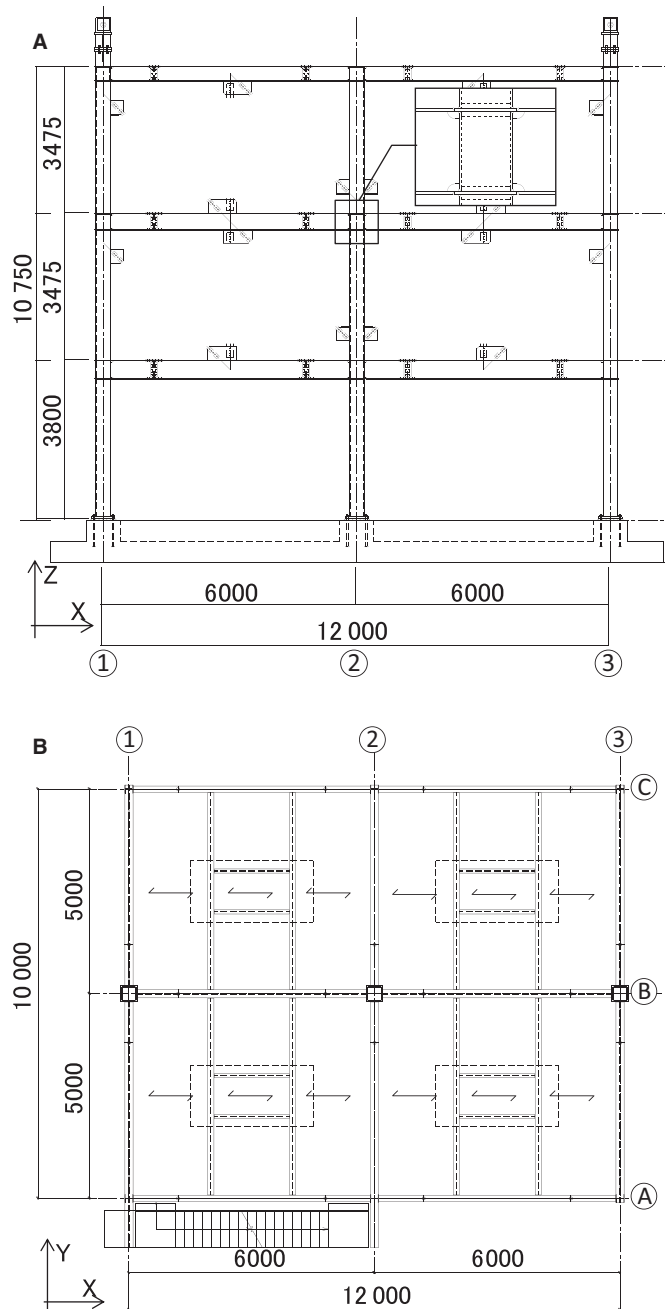**Figure 1.** Installation of specimen

Figure 2. Specimen for shaking-table test. (A) Framing plan (2F), (B) Framing elevation (B)

Table 1. Section list

	Column	Beam
RF	-	H-350 × 175 × 7 × 11
3F	B-350 × 350 × 9	H-400 × 200 × 8 × 13
2F	B-350 × 350 × 12	H-450 × 200 × 9 × 14
1F	B-350 × 350 × 12	-

scale inputs of JR-Takatori are shown in Figure 3. The story-shear force was evaluated as a product of the total mass above a floor and the corresponding floor-response acceleration. In the case using the 40% scale input of JR-Takatori, although a

slight nonlinearity can be seen at the first story, the overall structure behaved almost linearly, as shown in Figure 3A. The maximum story-drift ratio for each story reached 1/111-1/78, and tends to increase for lower floors. In this case, cracks were observed in the concrete slabs that were orthogonal to the excitation direction. Residual deformations of anchor bolts (2-3 mm) were also observed. In the case using the 60% scale input of JR-Takatori, nonlinear responses were clearly observed in a cycle when the maximum story-drift occurred on the first and second stories. For each floor, the maximum story-drift ratio reached 1/101-1/36. It appears that flanges at the beam ends on the second and third floors were plasticized because peelings of the mill scale were observed. The residual deformations of anchor bolts at the bottom of the columns reached 7.5-10 mm. For each floor, the maximum story-drift ratio reached 1/84-1/33 in the case of JR-Takatori 80%, which was comparable with that obtained from JR-Takatori 60%. However, in this case, nonlinear behaviors were observed in several cycles other than the cycle when there were maximum story-drifts. This showed that hysteretic energy absorptions were dispersed within a few cycles. In addition, fine ductile cracks were observed at the bottom of the scallop in the bottom flange of beams on the second floor that were connected to the exterior columns. Residual deformations of the anchor bolts at the bottom of the columns reached 9-11.5 mm. For the 100% scale input, with the full-scale acceleration of JR-Takatori, the maximum story-drift ratio for each story reached 1/47-1/13. On the second floor, fully opened cracks were observed at the bottom flanges of beam ends that were connected to the columns on lines 1 and 3. On the third floor, a fully opened crack and a partially opened crack were also observed at beam ends that were connected to columns on lines 3 and 1, respectively. The partially opened crack penetrated in the thickness direction, and the length of the crack in the width direction of the flange was about 70 mm. At those beams, local buckling of bottom flanges was also observed. The results illustrate the decrease in the story stiffness for each story, as shown in Figure 3D.

3. Finite-element analysis

3.1 Finite-element mesh

An outline of the analytical model is shown in Figure 4. In this study, the FE model was elaborated to replicate adequately entire shape of the specimen. All steel members were modeled with first-order planer elements that have 4-node at a unit length of 25 mm except for columns on the lines A and C. The planer elements had 4 integration points in the thickness direction and 1 integration point in the plane. The scallops were made to become single arc, whose radius was 35 mm, following the conventional approach used at the time of the Hyogoken-Nambu earthquake. The shape of the scallop was meshed at a unit length of 15 mm in order to divide the arc into 4 meshes. As the concrete parts, 8-node solid elements were used. In the model, beam elements were used as the reinforcement bar, headed stud, and anchor bolts. Beams and slabs were connected with headed studs, ie, flanges (shell elements) of beams shared their nodes with bottom nodes of studs (beam elements), and with the exception of the bottom nodes, the headed studs shared their nodes with those of slabs (solid elements). The number of elements and nodes was 2,186,644 and 2,134,151, respectively.

Contact conditions that are based on the penalty method were considered for parts that were actually in contact between separated members. In the model, slabs and columns, as well
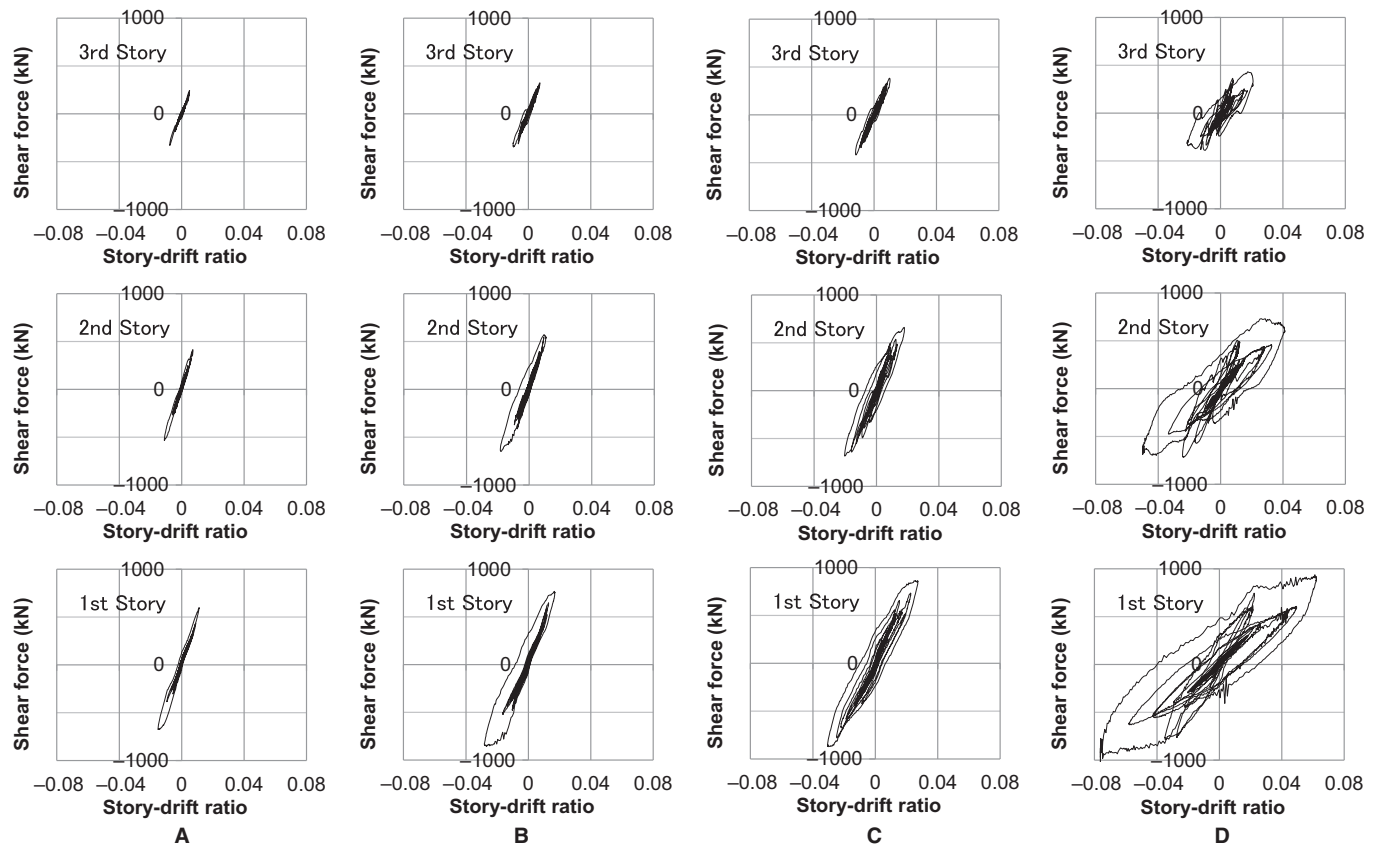
Figure 3. Hysteresis curve (experiment). (A) 40%, (B) 60%, (C) 80%, and (D) 100%

as slabs and flanges of beams and column bottom parts were in contact. At the bottom parts of the column, the contact condition was adopted as base plates of the columns and the foundation, and the base plates and nuts of anchor bolts, as shown in Figure 4C. The nuts were modeled as a rigid body.

3.2 Material models

A 2-surface model proposed by Yoshida and Uemori[14] was used for steel frame parts meshed by shell elements. The material properties of each member were determined from a material test that had been conducted before the shaking-table test, and results of cyclic material tests for SS400 were obtained from a previous study[15] because no cyclic material tests were conducted in these experiments. For the uniaxial loading test and cyclic loading tests, comparisons of analytical results and experimental results are shown in Figure 5. The yield plateau was ignored in the steel model, and the elastic material model was adopted to joist beams.

For concrete parts meshed by solid elements, the yielding surface proposed by Ottsen[16,17] was used during compression, and 3 orthogonal cracks could be formed in response to tensile principal stresses. The material properties of the concrete model were determined from a specified design-compressive strength. After crack initiation, the crack-normal stress was allowed to decay as a linear function of the crack-normal extension. The gradient of the decaying line was then determined from a tensile fracture energy of the concrete. The concrete material model used for the foundation was an elastic model as no damage was expected.

For the parts meshed by beam elements, the Ramberg-Osgood model was used.[18] The material properties of these members

were determined from the material tests. The linear isotropic elastic model was used for the parts that are unlikely to reach plastic region; columns on lines A and C, all joist beams, concrete foundation, and reinforcement bars in the foundation.

3.3 Analytical cases

The analytical cases conducted in this study are listed in Table 2. In this study, the analyses were carried out using a consecutive and sequential input motion that was continuously connected to 60%, 80%, and 100% scales of JR-Takatori as shown in Figure 6. Analytical cases were determined according to whether or not the fracture was considered during the phase using the 100% scale of JR-Takatori. In a previous study, it was reported that consideration of the seismic excitation history is important to simulate behaviors of shaking-table tests using consecutive seismic input motions.[19] Thus, 60% and 80% scales of JR-Takatori were considered as seismic excitation histories because nonlinear behaviors were not observed until the experimental case using the 40% scale of JR-Takatori, as mentioned in chapter 2. The phases of the 60% and 80% scales of JR-Takatori, which were considered as the excitation history, are called Case-60 and Case-80, respectively. A case that does not consider the fracture in the phase of the full-scale input of JR-Takatori is called Case-100, and a case that considers fracture in that phase is called Case-100-F.

A linear eigenvalue analysis was conducted to validate the analytical models in the linear range. The modeling of the column bottoms shown in Figure 4C was simplified, and nodes that were placed at the bottom of the columns were constrained in the eigenvalue analysis. The validation was conducted by comparing eigenvalues obtained by the analysis
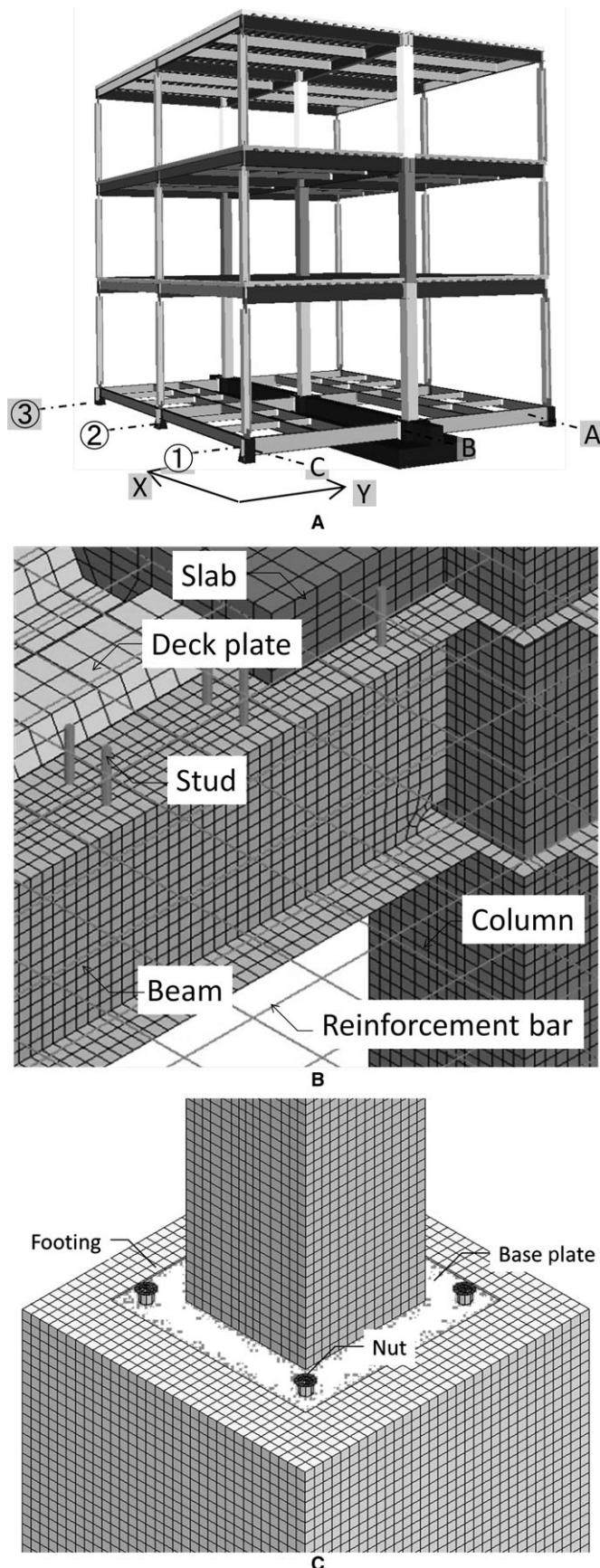
Figure 4. FE Model. (A) Whole view, (B) Detailed view (Joint Area), (C) Detailed view (Column Base)

with observed values. The observed natural frequencies were evaluated spectrum analyses of measured accelerations and story drifts under random waves (the maximum acceleration magnitude is 0.5 m/s² that were applied to the specimen before each seismic excitation.[20]

3.4 Considering fracture method and other analytical conditions

The fracture was considered by the forced elimination of elements in areas where the fracture actually occurred during the test at the times at which the fracture occurred at each part. A conceptual figure of the operation to remove elements is shown in Figure 7. The fracture of flanges of the beams was determined from close-up video footage, and damage observations were conducted after each experimental case. The fracture of the webs of the beams was assessed using only video footage. In the analysis, the elements were eliminated when cracks appeared to penetrate in the direction of the thickness and fine cracks were ignored. In addition, in this study, repeated contact of the fracture faces was ignored because the crack faces of the beam flanges were generated oblique to the axial direction of the beams, and behavior such as where one fractured end slid into the other end was observed.

The dynamic explicit scheme based on the central-difference method was used as the time-integration scheme. The FE analysis code LS-DYNA R.7.1.1 was used in this analysis. The time step used in the analysis was determined from the Courant condition with an initial time interval of 3.5×10^{-6} s. Analysis of the behavior took approximately 80 h under the seismic wave, as well as a set of sequential waves, ie, JR-Takatori 60%, 80%, and 100%, using 504 cores of a supercomputer (called Magnolia) located at the Institute for Information Management and Communication, Kyoto University, Japan.

3.5 Analytical results

Natural frequencies that were obtained by the eigenvalue analysis and evaluated by the spectrum analysis of responses under random waves are shown in Table 3. Modal shapes obtained from the analysis are shown in Figure 8. Only the analytical results in the excitation direction are shown in the table and figure. The natural frequencies evaluated by the eigenvalue analysis agreed with observed values of the actual specimen from the first to the third order. Therefore, the analytical model replicated adequately structural properties of the specimen in the linear range.

Time histories of the story-drift ratios for Case-60 and Case-80 are shown in Figures 9 and 10, respectively, while time histories of the story-shear force for those cases are shown in Figures 11 and 12, respectively. The times in the experimental cases are shown on the abscissa of those time histories, and times in the numerical analysis are shown in parentheses. The maximum values of the story-drift ratio obtained from Case-100 and Case-100-F are shown in Table 4. Root-mean-square error (RMSE) values of the story-drift ratio for analytical and experimental results in these cases are also shown in Table 4. The RMSE is expressed in the form of Equation (1). Time histories of the story-drift and story-shear force obtained form Case-100 and Case100-F are shown in Figures 13 and 14, respectively. Values on the horizontal axes are written in the same way as in Figures 9–12.

$$\text{RMS} = \sqrt{\frac{1}{N} \sum (x_{\text{EXP}} - x_{\text{ANL}})^2} \qquad (1)$$

where N: Number of data, x_{EXP}: experimental result of story-drift ratio, and x_{ANL}: analytical result of story-drift ratio.
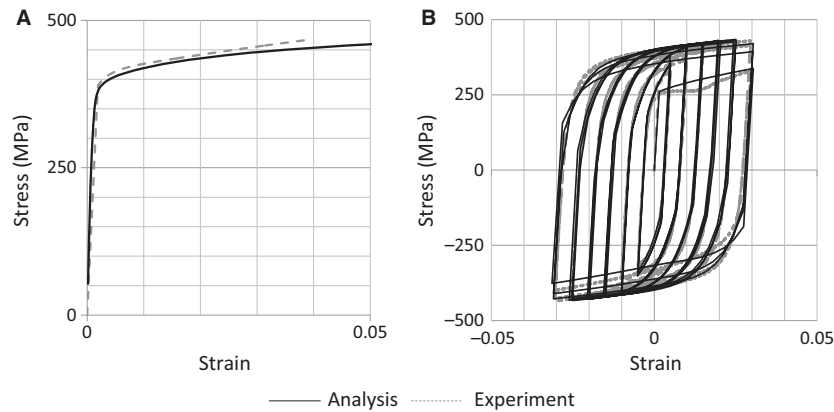
Figure 5. Steel material model. (A) Monotonic (1,2F Column), (B) Cyclic[15]

Table 2. Analysis cases

Case	Case-60	Case-80	Case-100	Case-100-F
Input	JR-Takatori 60%	JR-Takatori 80%	JR-Takatori 100%	
History	Not considered	Considered		
Fracture	Not considered			Considered

Table 3. Natural frequency (Hz)

	First	Second	Third
Observed	1.57	4.85	8.58
Analysis	1.58	4.84	8.75

Figure 6. Excitation

$$\varepsilon_p^{\text{eff}} = \int d\varepsilon_p, \; d\varepsilon_p = \sqrt{\frac{2}{3} d\varepsilon_{ij}^p d\varepsilon_{ij}^p} \tag{2}$$

where $\varepsilon_p^{\text{eff}}$: equivalent plastic strain, $d\varepsilon_p$: equivalent plastic strain increment, and $d\varepsilon^p{}_{ij}$: each component of the plastic strain increment tensor.

In Case-60 and Case-80, which analytically used 60% and 80% scale inputs of JR-Takatori as excitation histories, both the story-drift ratio and shear force showed good agreement with the experimental results. Therefore, the analytical model can replicate the shaking-table test before applying the full-scale JR-Takatori input.

As shown in Table 4, the RMSE shows that the errors of the analytical and experimental results in Case-100-F are less than those of Case-100 in all stories. It appears that consideration for the fracture improves the accuracy of analysis. In addition, with the exception of the third story, the errors in the maximum values of the story-drift ratio decrease when the fracture is considered. After 14 s (indicated as (v) in Figure 13D), the analysis that does not consider the fracture underestimates the story drift and exhibited a phase delay of the time histories.
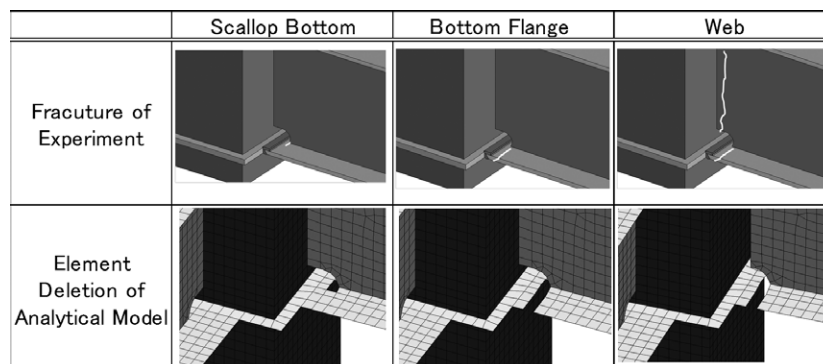
The timings of fractures in the experiment are denoted in Figure 13D using the values of Table 5. For each part, the states of the fracture are shown in Table 5. In Table 5, brief explanation of appearances at the fracture part, video footage of the fracture observed during the experiment and the states of elimination of elements in the analysis are shown. Contours in the analysis results represent the effective plastic strain expressed in the form of Equation (2):

Figure 7. Conceptual figure of fracture modeling

Figure 8. Eigen modal shape

Figure 9. Story-drift ratio history (Case-60) (——Analysis; ······Experiment). (A) First Story, (B) Secondn Story, (C) Third Story
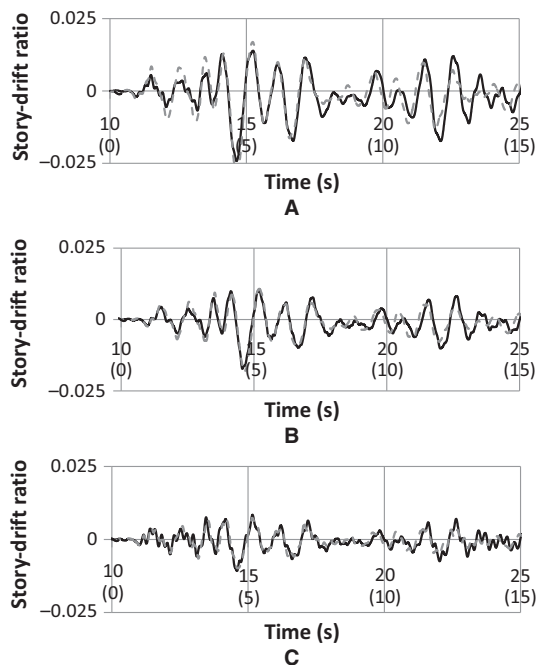

Figure 10. Story-shear force history (Case-60) (——Analysis; ······Experiment). (A) First Story, (B) Second Story, (C) Third Story

As shown in Table 5, the bottom flanges of beam ends that were connected to columns on lines 1 and 3 were fully fractured at a time indicated in Figure 13D as (iv). Therefore, it appears that the analytical model in Case-100, in which the fracture was not considered, could not replicate the actual behavior of the specimen after 14 s. The phase delay can also be seen in the time histories of the story-shear force after 15 s as well as those of the story-drift ratio. In Case-100-F, an improvement in the precision can be seen for both the story-drift ratio and shear force. Therefore, an improved analysis after fracture was obtained by the forced elimination of the elements that were placed in positions where the fracture occurred in the experiment, and at the times when the fractures were observed.

The plastic strain concentration on the bottom of the scallops can be seen in Table 5; therefore, the strain concentration on the bottom of scallops that appeared to occur in the experiment was reproduced by the analysis. In Table 5 (iv)-(viii), it can be seen that local buckling of the bottom flange of the beams occurred in the experiment. On the other hand, local buckling in the analysis also occurred at the place corresponding to the experiment. In addition, the analysis replicated the behavior of the experiment with respect to the deformation.
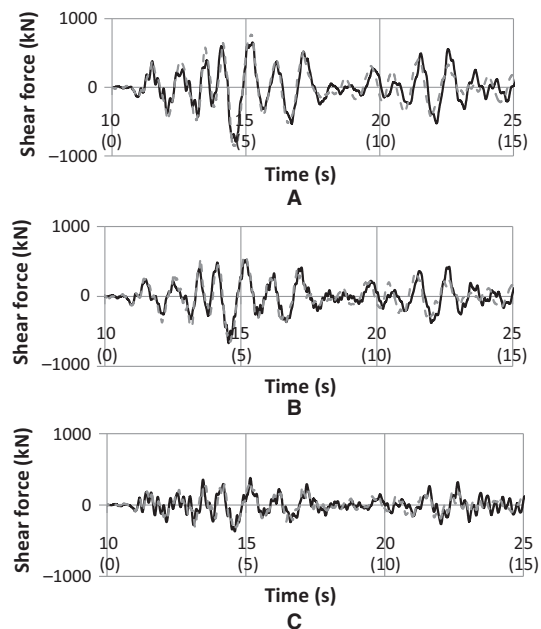
4. Cumulative damage at fractured parts

In this section, a study about damage that accumulates until a fracture occurs is presented. Some models were proposed for the fracture of steel members caused by low-cycle fatigue, and they are roughly divided into 2 types. One type is defined based on the relationship between the ductility factor of members and the number of cycles, while the other type is defined from the relationship between the plastic strain amplitude and the number of cycles. The latter type is the focus of this study because the specimen was modeled using shell elements, and local strain can be observed.

4.1 Method of evaluating damage

The Manson-Coffin law is often used to express the characteristic of the low-cycle fatigue life of steel materials.[21] The Manson-Coffin law is expressed as in Equation (3).

$$\tilde{\varepsilon}_p \times N^\alpha = C \tag{3}$$

where $\tilde{\varepsilon}_p$: the reversal plastic strain amplitude, N: number of cycles to failure corresponding to the reversal plastic strain, and C, α: material constants.
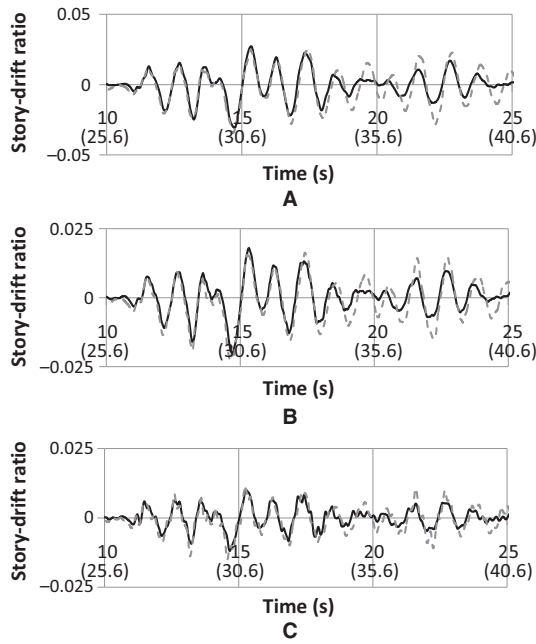
Figure 11. Story-drift ratio history (Case-80) (——Analysis; ┈┈┈Experiment). (A) First Story, (B) Second Story, (C) Third Story
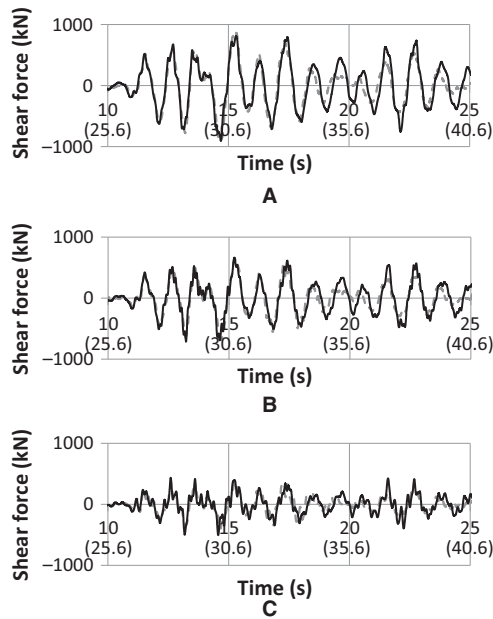

Figure 12. Story-shear force history (Case-80) (——Analysis; ┈┈┈Experiment). (A) First Story, (B) Second Story, (C) Third Story

In addition, the cumulative damage of a material under variable loadings is expressed using Minner's rule, which is expressed as Equation (4).[21]

$$D = \sum_{i=1}^{k} \frac{n_i}{N_i} \quad (4)$$

where D: cumulative damage, n_i: number of contributing cycles associated with the i-th reversal plastic strain amplitude $\tilde{\varepsilon}_{p,i}$ ($1 \leqq i \leqq k$), N_i: number of cycles to failure at the associated i-th reversal plastic strain amplitude.

Table 4. Maximum value and RMSE of story-drift ratio

Story		First	Second	Third
Max.	Exp.	0.076	0.050	0.021
	Case-100	0.062	0.039	0.024
	Case-100-F	0.087	0.059	0.029
RSME	Case-100	0.021	0.013	0.007
	Case-100-F	0.010	0.008	0.005

It is hypothesized that when the cumulative damage D of an element reaches 1.0, the element fails. In order to count the contributing number of cycles associated with each of the plastic strain amplitudes, cycle-counting methods such as the rainflow counting method are used.[22] There is some difficulty in treating the cycle-counting methods in transient response analyses. This is because the cycles n_i and ranges of plastic strain amplitudes $\tilde{\varepsilon}_{p,i}$ need to be discrete values. In addition, a large calculation load is required in analyses using large-scale models such as those used in this study because the histories of the strain paths of all the elements need to be stored. On the contrary, Xue proposed a method to treat the Manson-Coffin law and the Minner's rule with continuous variables.[23,24] This study follows that approach, and quantifies the damage to the fractured parts.

Consider a case where a material fails under a monotonic loading path, ie, $\tilde{\varepsilon}_{p0} = \tilde{\varepsilon}_p$ and $N = 1/2$. By substituting these values into Equation (3), the relationship between $\tilde{\varepsilon}_{p0}$ and C is expressed as Equation (5).

$$\tilde{\varepsilon}_{p0} \cdot 2^{-\alpha} = C \quad (5)$$

For each half cycle of the i-th plastic strain amplitude $\tilde{\varepsilon}_{p,i}$, the damage increment ΔD_i associated with the strain amplitude $\tilde{\varepsilon}_{p,i}$ is expressed by Equation (6) using Equation (4).

$$\Delta D_i = \frac{1}{2N_i} \quad (6)$$

From Equations (3), (5), and (6), ΔD_i is rewritten as Equation (7).

$$\Delta D_i = \left(\frac{\tilde{\varepsilon}_{p,i}}{\tilde{\varepsilon}_{p0}}\right)^{1/\alpha} = \left(\frac{\tilde{\varepsilon}_{p,i}}{\tilde{\varepsilon}_{p0}}\right)^m \quad m = \frac{1}{\alpha} \quad (7)$$

Equation (7) gives the cumulative damage, such as a step function under the half-cycle monotonic loading path. Now, the cumulative damage is expressed in the form of a continuous function. The cumulative damage function is also defined as $\psi(\varepsilon_p^*)$, which is associated with an arbitrary plastic strain amount ε_p^* along a monotonic loading path. $\psi(\varepsilon_p^*)$ is assumed to be defined as Equation (8), which is in a similar form to Equation (7).

$$\Psi\left(\varepsilon_p^*\right) = \left(\frac{\varepsilon_p^*}{\tilde{\varepsilon}_{p0}}\right)^m \quad (8)$$

where $\varepsilon_p^* = \sqrt{2/3\varepsilon_{ij}^p \varepsilon_{ij}^p}$ and ε_{ij}^p: each component of the plastic strain tensor.

It should be noted that the value of ε_p^* is different from the effective plastic strain ε_p^{eff} defined as Equation (2), which is the accumulated value of the effective plastic strain increment. The damage increment associated with the plastic strain
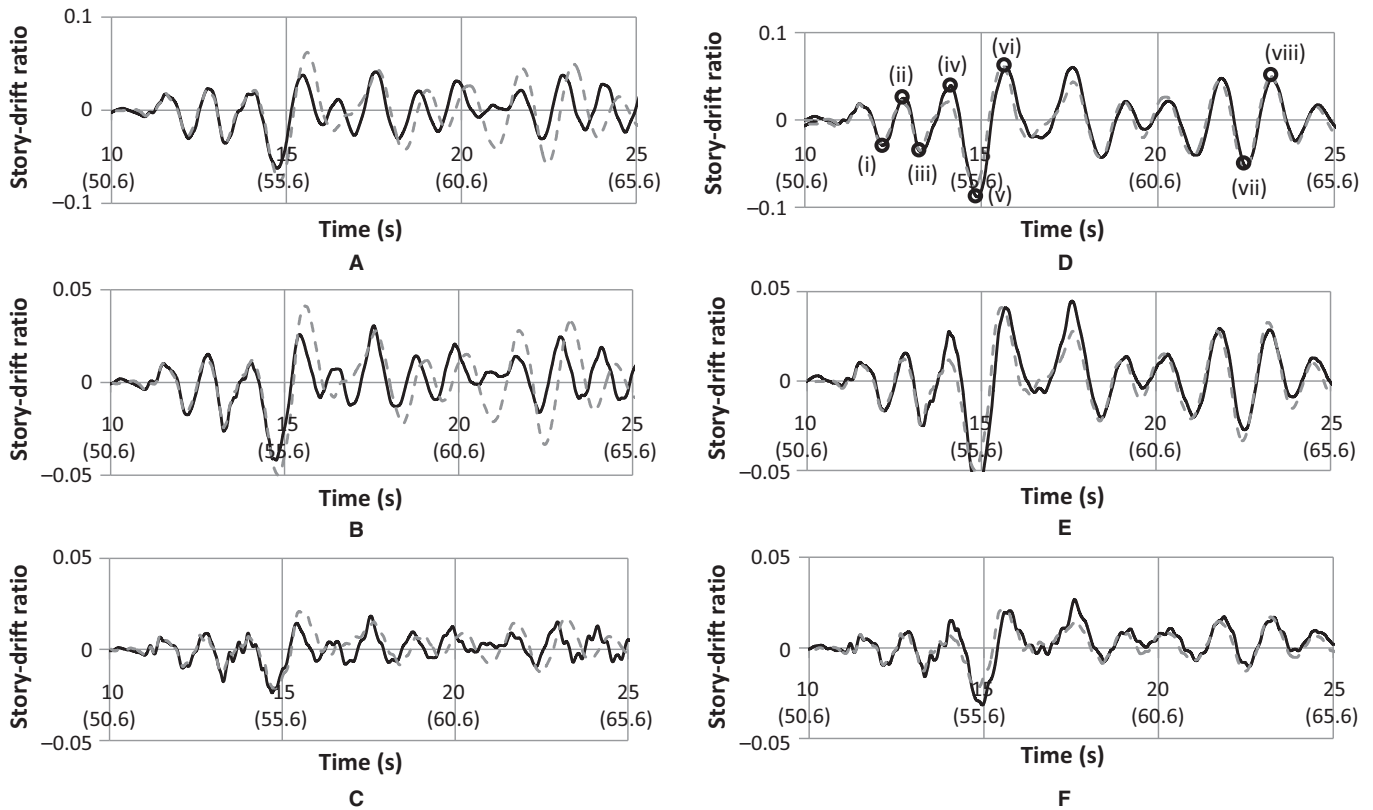
Figure 13. Story-drift ratio history (Case-100, Case-100-F) (——Analysis; ‑‑‑‑Experiment). (A) First Story (Case-100), (B) Second Story (Case-100), (C) Third Story (Case-100), (D) First Story (Case-100-F), (E) Second Story (Case-100-F), (F) Third Story (Case-100-F)
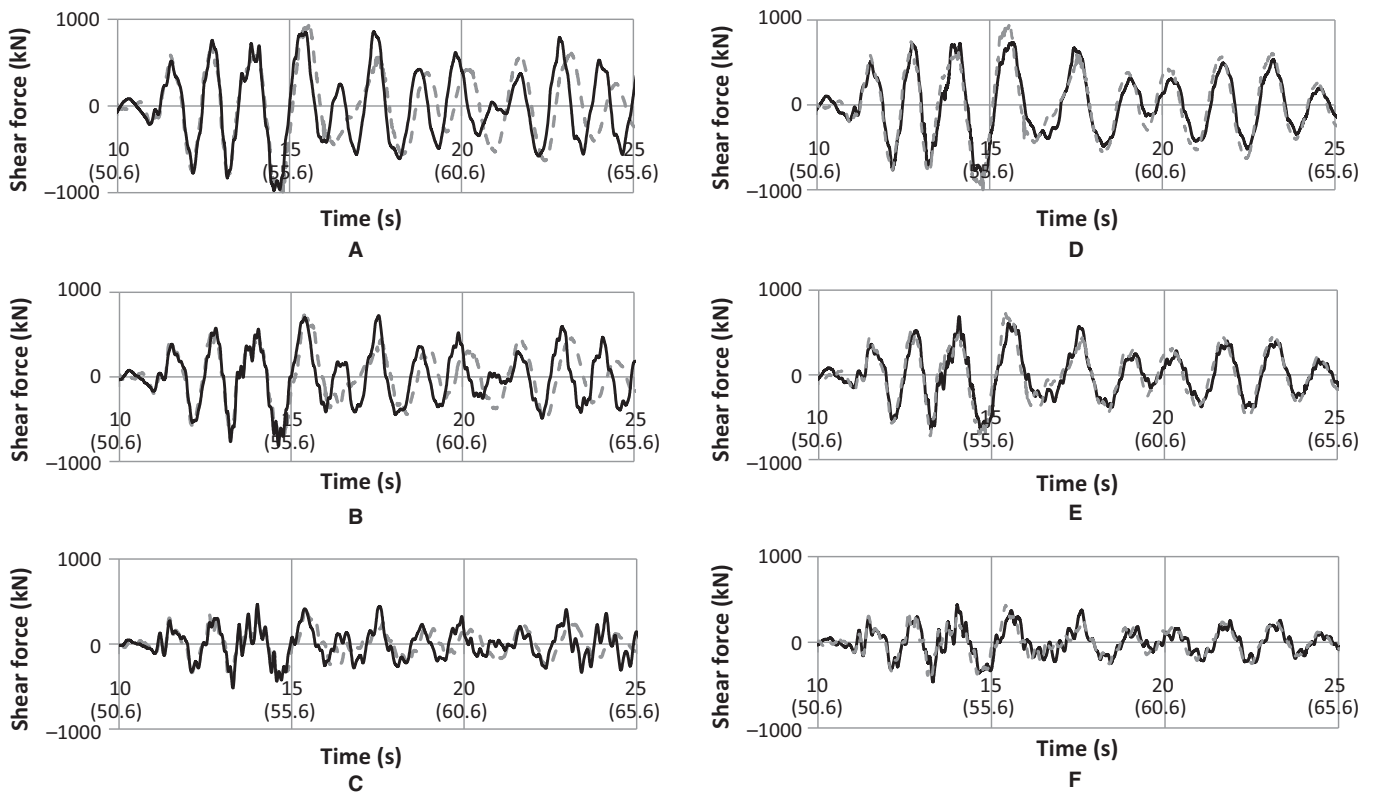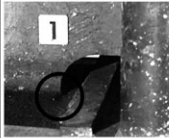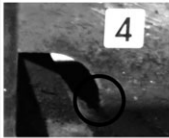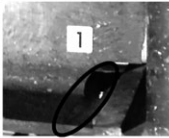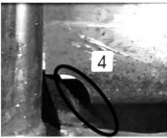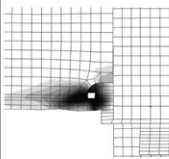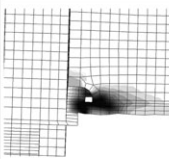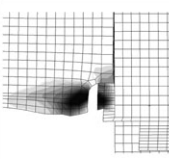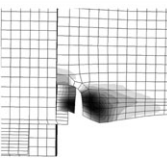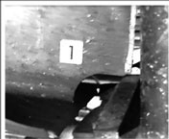

Figure 14. Story-shear force history (Case-100, Case-100-F) (——Analysis; ‑‑‑‑Experiment). (A) First Story (Case-100), (B) Second Story (Case-100), (C) Third Story (Case-100), (D) First Story (Case-100-F), (E) Second Story (Case-100-F), (F) Third Story (Case-100-F)

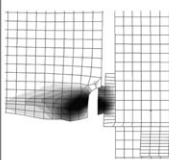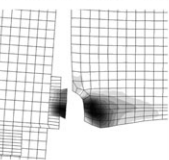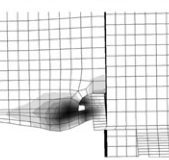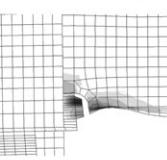**Table 5.** State of fracture (effective plastic strain [0.0 ⟶ 1.2])

	(i)	(ii)	(iii)	(iv)
Briefing of Fracture State	A crack was detected on the scallop bottom at ①-2F	A crack on the scallop bottom at ③-2F penetrated the flange (10 mm)	Bottom flange at ①-2F fully fractured	Bottom flange at ③-2F had fully fractured
Experiment				
Analysis				

	(v)	(vi)	(vii)	(viii)
Briefing of Fracture State	Web at ①-2F fractured.	Web at ③-2F fractured. Crack on the scallop bottom at ③-3F penetrated the flange (3 mm)	Crack on the scallop bottom at ①-3F penetrated the flange (3 mm)	Bottom flange at ③-3F fully fractured
Experiment				
Analysis				

increment $d\varepsilon_p$ should be defined as the derivative of Equation (8), so that when ε_p^* increases from 0.0 to $\tilde{\varepsilon}_{p,i}$, the damage is equal to the value given by Equation (7). Therefore, the damage increment is defined as Equation (9).

$$\frac{d\Psi\left(\varepsilon_p^*\right)}{d\varepsilon_p} = \frac{d\Psi\left(\varepsilon_p^*\right)}{d\varepsilon_p^*}\frac{d\varepsilon_p^*}{d\varepsilon_p} = m\left(\frac{\varepsilon_p^*}{\tilde{\varepsilon}_{p0}}\right)^{m-1}\frac{1}{\tilde{\varepsilon}_{p0}}\left(\frac{d\varepsilon_p^*}{d\varepsilon_p}\right) \quad (9)$$

It is assumed that by Xue,[23,24] the damage monotonically increases during plastic deformation regardless of any increase or decrease of ε_p^*. According to the definition of ε_p^* and Equation (2), $d\varepsilon_p^*/d\varepsilon_p$ is equal to 1.0 when ε_p^* increases, and it is -1.0 when ε_p^* decreases. Therefore, the cumulative damage D is defined as the integrated value of an absolute value of $d(\varepsilon_p^*)$ along all plastic strain paths, as shown in Equation (10).

$$D = \int |d\Psi(\varepsilon_p^*)| = \int m\left(\frac{\varepsilon_p^*}{\tilde{\varepsilon}_{p0}}\right)^{m-1}\frac{1}{\tilde{\varepsilon}_{p0}}d\varepsilon_p \quad (10)$$

4.2 Identification of material constants for damage evaluation
Equations (3) and (10) have 2 material constants. Now, we determine the material constants from the result of a component test conducted before the shaking-table test[25] and the relationship of those constants which is reported in the reference.[21] The determined constants are used to quantify the cumulative damage of the fractured parts.

A conceptual diagram of the component test is shown in Figure 15. The specimen of the component test is made to reproduce an exterior beam-column joint on the second floor of the specimen for the shaking-table test. Then, a cyclic and increasing load was imposed on the tip of the beam. The distances between supporting points of the column and from the center of the column to the loading point were 3000 mm. For the beam and welding wire, the material used was the same as that of the specimen for the shaking-table test.

An analytical model for the component test is shown in Figure 16. The model was meshed at a unit length of 25 mm, as was the case with the analytical model for the shaking-table test. The model for the installation parts was omitted, and the steel members and supporting or loading points were connected by rigid bodies. The same material models were used with the analysis for the shaking-table test; however, the fracture was not considered. The damage at the fractured part was evaluated by extracting ε_p^* and $d\varepsilon_p$ in Equation (10) from component analysis.
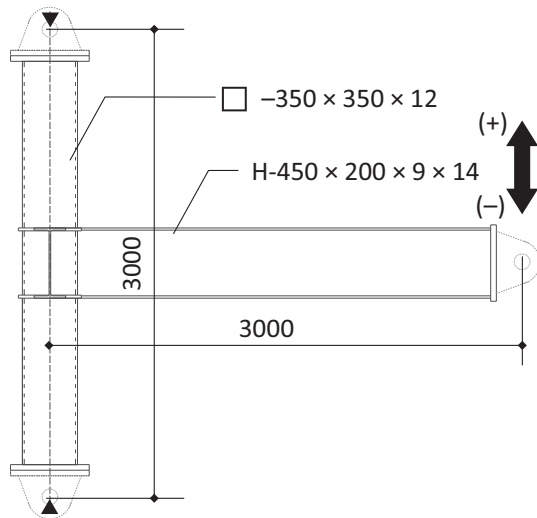
Figure 15. Specimen (component test)

Figure 17. Results of component test

The relationships between the bending moment and rotational angle of the beam obtained from both the component analysis and the experiment are shown in Figure 17. The analytical result agreed well with that of the experiment. Therefore, it is confirmed that $\varepsilon_p{}^*$ and $d\varepsilon_p$ obtained from the component analysis can be used in order to identify the material constants.

Saeki et al. reported that the relationship between the 2 material constants is approximated by an exponential function.[21] The 2 material constants are expressed as C and α in Equation (3), and as m and $\tilde{\varepsilon}_{p0}$ in Equation (10). Then, including the results of experiments which were conducted by Nakagome et al. and Harayama et al. to the result reported in Ref. [21], as shown in Figure 18, the relationship between the 2 material constants is rewritten as Equations (11) and (12):

$$C = 1.693 \times 716.9^{\alpha} \qquad (11)$$

$$\tilde{\varepsilon}_{p0} = 0.0169 \times 1433.8^{1/m} \qquad (12)$$

From the above, m and $\tilde{\varepsilon}_{p0}$ are evaluated using the history variables obtained from the component analysis and
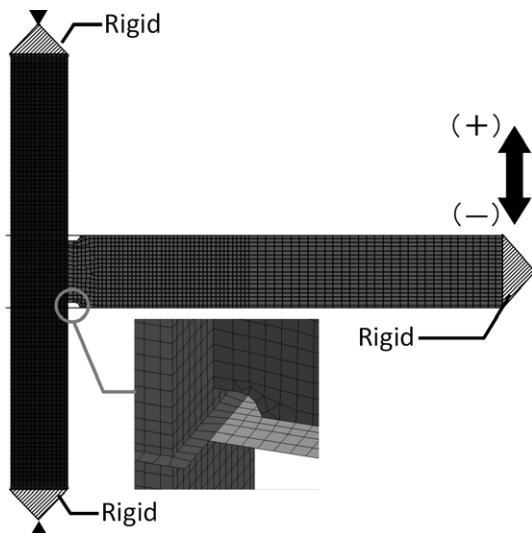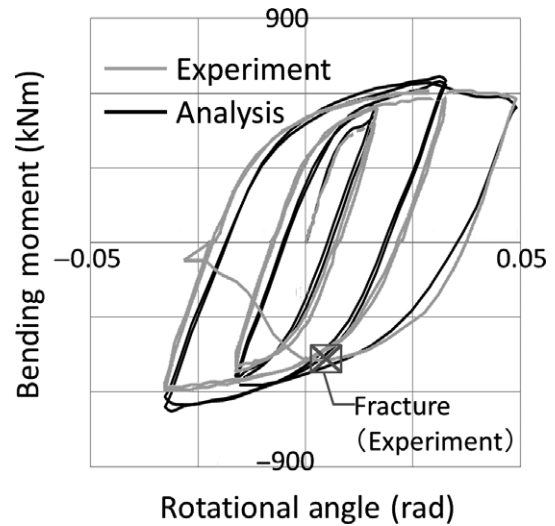
Equation (12) in the form of Equation (13), as follows:

$$\tilde{\varepsilon}_{p0} = 2^{\alpha} \times C = 0.16, \quad m = \frac{1}{\alpha} = 3.19 \qquad (13)$$

4.3 Time history of damage evaluation at fractured parts

Time histories of the damage evaluated from Case-100-F with Equation (10) are shown in Figure 19. The histories of the damage are displayed until just before the fracture, as shown in Figure 19. The horizontal axis of the time histories represents the analytical time, including the cases using 60% and 80% scales of JR-Takatori as excitation histories. Each end of the time histories represents the times at which elements are deleted. "Scallop bottom" and "Bottom of beam flange" shown in Figure 19 indicate the damage at the flange elements connected to the scallops and the outermost elements in the flange-width direction, respectively.

In the 60% phase, there was slight damage at the beam on the second floor. In this phase, the number of cases of damage
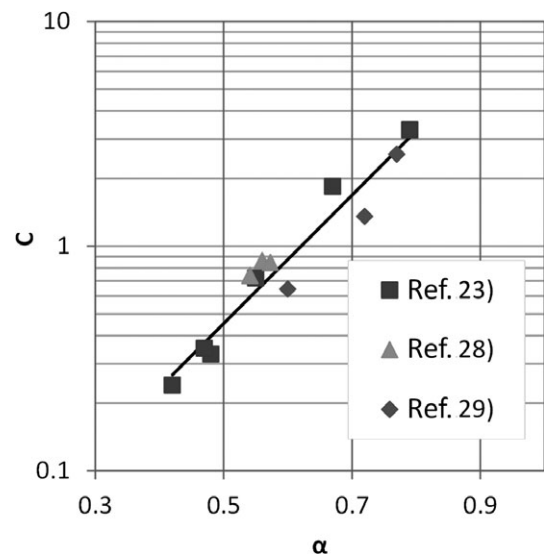

Figure 16. FE Model (component test)
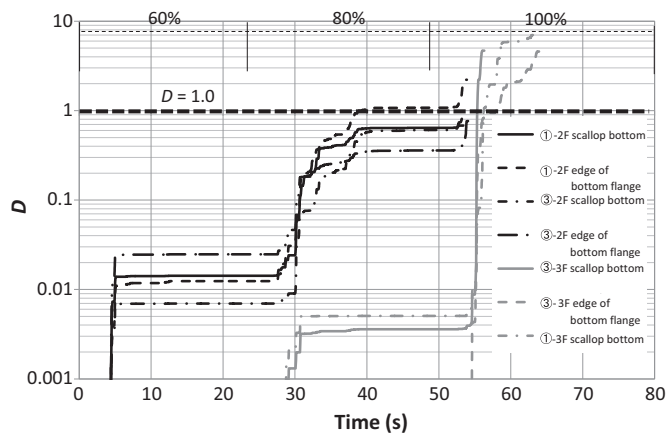

Figure 18. C-α diagram

Figure 19. Time history of damage

increased only once at around 5 s, which is consistent with the fact that nonlinearity was observed at the 1 cycle in which the maximum response occurred.

In the 80% phase, damage to the flanges of beams on the second floor increased rapidly at around 30 s, and damage to the beams on the third floor level began to accumulate. Then, nonlinearity was observed for the first and second stories. The times at which the nonlinearities were observed was in close agreement with the times at which the damage increased. The damage D at the second floor beams were within the range 0.36–1.06. While in the experiment, fine cracks were observed at the corresponding parts, full fractures were not observed at the beam flange. The observed fine cracks in the test suggest that the flanges of the beams were at the edges of fractures. This is in agreement with the obtained damage-time histories, which reflect the actual state of the damage in the test.

In the 100% phase, the fracture at the beam ends on the second floor was observed between 53 s and 55 s in the test. The fracture on the third floor was observed between 56 s and 64 s, ie, after the fracture on the second floor. Meanwhile, the damage D at the beams on the second floor was within the range 0.68-0.93 and 2.01. In other words, the damage exceeded 1.0 or was almost 1.0 at the times at which fractures were observed in the test. In addition, all of the damage histories show sharp increases just before the fractures. On the third floor, although the damage histories of the beams were less than 0.01 before the fractures on the second floor, those instances of damage also increased sharply after the second floor, and eventually exceeded 1.0. Therefore, the damage histories on the second and third floors are in agreement with the states of the fracture in the shaking-table test.

5. Conclusions

In this study, nonlinear analysis was performed using the detailed FE model that was meshed at a unit length of 25 mm for the full-scale shaking-table test of the steel frame, which resulted in cumulative damage by multiple strong motions. In conclusion, the study is summarized as follows.

1. The analysis was performed using a consecutive and sequential input motion, 60%, 80%, and 100% scales of JR-Takatori for the shaking-table test without considering fractures. The analysis could replicate adequately the responses of the experimental cases using the 60% and 80% scales of JR-Takatori. However, because the analysis

did not consider fractures, it could not replicate the responses of the experimental case of the full-scale JR-Takatori input after fracturing. The differences in the story-drift magnitudes and phase shifts were observed in the time histories of the story drift and shear force after the fracture.

2. An analysis that considers the fracture was also performed. The fracture was considered by removing the elements according to the actual timing of the fractures in the experiment at each part. As a result, the errors in the story drifts between experimental and analytical results in all stories decreased compared to those obtained from the analysis that did not consider the fracture. The phase delay of the time histories for the story-shear force was also improved. This additional operation resulted in an improvement in the reproducibility of the experimental responses after the fracture.

3. The damage index was introduced based on the Manson-Coffin law and the Minner's rule. The accumulated damage of the elements that were eliminated to reproduce the fracture was evaluated. The 2 material constants in the damage index were given by the estimative approximation based on the past experiments, thus, those material constants were determined by this approximation for this study. The actual material parameters are taken from the component test before the shaking-table test.

The histories of the damage index, which were evaluated at each fractured part, were shown to correlate to the appearance of the actual state of the fracture in the shaking-table test.

Disclosure

The authors have no conflict of interest to declare.

References

1 Kim Y, Kabeyazawa T, Matsumori T, Kabeyazawa T. Simulated earthquake test on a full-scale six-story reinforced concrete building at E-Defense – Part 11: 3-Dimensional Dynamic Analysis. *Summaries of Technical Papers of Annual Meeting AIJ*, C-2, pp. 393–394; 2007 (In Japanese).

2 Suita K, Matsuoka Y, Yamada S, Shimada Y, Tada M, Kasai K. Experimental procedure and elastic response characteristics of shaking table test – Dynamic collapse test of full-scale 4-story steel building part 1. *J Struct Constr Eng (Transaction of AIJ)*. 2009;**74**:157-166 (In Japanese).

3 Yamada S, Suita K, Matsuoka Y, Shimada Y. Elasto-plastic responses and process leading to a collapse mechanism – Dynamic collapse test of full-scale 4-story steel building part 2. *J Struct Constr Eng (Transaction of AIJ)*. 2009;**74**:1851-1859 (In Japanese).

4 Horimoto A, Tada M, Tamai H, Ohgami K, Kuwahara S, Mitani A. Three dimensional analytical simulation of collapse by collaborative structural analysis for full-scale 4-story steel building. *J Struct Eng*. 2009;**55B**:277-283. (In Japanese).

5 Shugyo M, Shimazu M. Elastoplastic seismic response analysis of a frame with lumped mass modeling by the fibered plastic hinge method. *J Struct Constr Eng (Transaction of AIJ)*. 2014;**79**:275-283 (In Japanese).

6 Hikino T, Ohsaki M, Kasai K, Tada M, Nakashima M. Summary of blind analysis contest for full-scale four-story steel building and evaluation of accuracy of numerical analysis. *J Struct Constr Eng (Transaction of AIJ)*. 2010;**75**:1717-1726 (In Japanese).

7 Ohsaki M, Katsura M, Watanabe H, Hikino T. Identification of analysis parameters using results of full-scale test and evaluation of variation of steel frame. *J Struct Eng*. 2013;**59B**:201-209. (In Japanese).

8 Yamashita T, Miyamura T, Hori M, Kajihara K, Ohsaki M, Kohiyama M, Akiba H. High-precision finite element analysis of shaking-table test on full-scale 4-story steel frame using e-simulator. Summaries of Technical Papers of Annual Meeting AIJ, Structure-I, pp. 333-334; 2012 (In Japanese).

9 Morikawa S, Taga K, Fukuoka T, Namba H, Shiraga S, Kajihara K. E-defense shaking table test for full scale steel building on cumulative damage by sequential strong motion – Part 3 shaking table test. Summaries of Technical Papers of Annual Meeting AIJ, Structure-III, pp. 979–980; 2014 (In Japanese).

10 Mizushima Y, Mukai Y, Namba H, Saruwatari T. Numerical simulation of a full-scale table test using detailed FEM model. Proceedings of the Conference on Computational Engineering and Science, Vol. 19, C-11-1; 2014 (In Japanese).

11 Takahashi M, Sawamoto Y, Kubota J, Kiyokawa T, Koshika N, Suzuki Y, Suita K, Koetaka Y, Iyama J, Nagae T. Planning of shaking table test using the e-defense – Quantification of collapse margin of steel high-rise buildings (part 2). Summaries of Technical Papers of Annual Meeting AIJ, Structure-III, pp. 969–970; 2013 (In Japanese).

12 Takatsuka K, Suita K, Umeda T, Takahashi M. Time history analysis considering degradation and fracture by crack propagation about shaking table test – Quantification of collapse margin of steel high-rise buildings (part 7). Summaries of Technical Papers of Annual Meeting AIJ, Structure-III, pp. 1241–1242; 2014 (In Japanese).

13 Takehara S, Nakashima M, Kanao I. Damage and collapse behavior of full-scale three-story moment frame subjected to cyclic loading – part 6: analysis considering fracture of members. Summaries of Technical Papers of Annual Meeting AIJ, C-1, pp. 981–982; 2004 (In Japanese).

14 Yoshida F, Uemori T. A constitutive equation for description of large-strain cyclic plasticity. *Trans Japan Soc Mech Eng (A)*. 2002;**68**:415-421 (In Japanese).

15 Sadasue K, Kasai K, Ono Y, Kaneko H, Yamazaki H. Curved hysteresis model of structural steel under cyclic loading – part 2 experimental work and verification of analytical model. Summaries of Technical Papers of Annual Meeting AIJ, C-1, pp. 747–748; 2005 (In Japanese).

16 Wai F. Chen: plasticity in reinforced concrete, Maruzen; 1985.

17 Broadhouse BJ. The Winfrith concrete model in LS-DYNA3D. Report: SPD/D(95)3, Structural Performance Dept., AEA Technology, Winfrith Technology Centre, UK; 1995.

18 JSOL Corporation. LS-DYNA keyword user's manual volume 2. 2012 (In Japanese).

19 Mizushima Y, Mukai Y, Namba H, Taga K, Saruwatari T. Detailed FEM analysis considering the excitation history for full scale shaking table test applying multiple times seismic excitations. *J Japan Assoc Earthq Eng*. 2016;**16**:1_217-1_227 (In Japanese).

20 Shimomura H, Irie C, Mukai Y, Namba H. E-defense shaking table test for full scale steel building on cumulative damage by sequential strong ground motion – Part 5 structural monitoring and estimation for damaging progression with shaking table test response. Summaries of Technical Papers of Annual Meeting AIJ, Structure-III, pp. 983–984; 2014 (In Japanese).

21 Saeki E, Sugisawa M, Yamaguchi T, Mochizuki H, Wada A. A study on low cycle fatigue characteristics of low yield strength steel. *J Struct Constr Eng (Trans AIJ)*. 1995;**472**:139-147 (In Japanese).

22 Japanese Society of Steel Construction. Fatigue Design Recommendations for Steel Structure, Gihodoshuppan; 2012 (In Japanese)

23 Xue L. Damage accumulation and fracture initiation in uncracked ductile solids subject to triaxial loading. *Int J Solids Struct*. 2007;**44**:5163-5181.

24 Xue L. A unified expression for low cycle fatigue and extremely low cycle fatigue and its implication for monotonic loading. *Int J Fatigue*. 2008;**30**:1691-1698.

25 Fukuoka T, Morikawa S, Namba H. E-defense shaking table test for full scale steel building on cumulative damage by sequential strong motion – Part 2 subassemblage tests. Summaries of Technical Papers of Annual Meeting AIJ, Structure-III, pp. 977–978; 2014 (In Japanese)

26 Disaster Management, Cabinet Office, Government of Japan. Report of the seismic intensity distribution and tsunami height due to the Nankai trough huge earthquake (first report); 2012.

27 Suita K, Tanaka T, Sato A, Manabe Y, Tsukada T, Su Z. Effect of ultimate flexural strength of beam end connection on deformation capacity – Deformation capacity of welded beam-to-column connection subjected to repeated plastic strain part 1. *J Struct Constr Eng (Trans AIJ)*. 2011;**76**:1135-1142 (In Japanese).

28 Nakagomi T, Iwamoto T, Kamura H, Shimokawa H, Harayama K. Experimental study on fatigue characteristic of flat-bar brace with low yield stress steel stiffened by square steel tube. *J Struct Constr Eng (Trans AIJ)*. 2000;**530**:155-161 (In Japanese).

29 Harayama K, Nakagomi T, Horie T. Experimental study on fatigue characteristic of material for hysteretic damper. Summaries of Technical Papers of Annual Meeting AIJ, C-1, Structure-III, pp. 505–506, 2004 (In Japanese).